

WIND TUNNEL AERO-HEATING AND MATERIAL DESTRUCTION TESTS FOR IMPROVED DEBRIS RE-ENTRY ANALYSIS

G. Koppenwallner ⁽¹⁾, T. Lips ⁽²⁾, D. Alwes ⁽³⁾

⁽¹⁾ HTG- Hypersonic Technology Göttingen, 37191 Katlenburg –Lindau, Germany, Email: g.koppenwallner@htg-hs.de

⁽²⁾ HTG- Hypersonic Technology Göttingen, 37191 Katlenburg –Lindau, Germany, Email: t.lips@htg-hst.de

⁽³⁾ DLR Deutsches Zentrum für Luft und Raumfahrt, Bonn-Oberkassel, Germany, Email: d.alwes@dlr.de

ABSTRACT

During the S/C re-entry destruction fragments of irregular geometry are released. One finds spheres, boxes and cylinders, which may be hollow and which are flying in tumbling motion. The experimental database on such bodies is limited. Therefore heat transfer test have been conducted in the hypersonic vacuum wind tunnel V2G of DLR Göttingen. With a special model support also rotating models could be tested.

Another study objective was the thermal destruction of selected materials and CFRP components under simulated re-entry heat loads. In use are solid CFRP structures, honeycombs with CFRP facesheets, or thin walled titanium tanks with external CFRP reinforcements. The destruction of multilayer structures may be completely different to solid thick CFRP. Therefore samples of 12 CFRP and CFRP honeycombs have been tested in the LBK 2 arc jet facility of DLR.

1. INTRODUCTION

In order to conduct a re-entry destruction analysis with a multidisciplinary code like SCARAB [1],[2] the analysis models for individual disciplines like aero-heating or thermal destruction should be as realistic as possible and validated against experiments. Our past experience showed that the destruction of multilayer structures consisting of CFRP and metal components like aluminium honeycombs or internal titanium shells can not be treated with simple thermal melting models.

We therefore could with support of DLR initiate experimental wind tunnel and arc jet tests. The tests addressed the heat transfer to irregular shaped bodies and the thermal destruction of CFRP structures [3].

A second task was to provide a database for the improvement of the heat load modelling in SCARAB.

2. MODELS, FACILITY FOR HEATING TESTS

The main task of the wind tunnel tests was to investigate the integral heat transfer to typical construction elements of spacecraft with the following shapes: sphere, circular and rectangular cylinders.

The surface integrated heat transfer rate Q' can be determined from the temperature time response of a solid calorimeter model [4] suddenly exposed to the flow. This can be achieved with copper models of limited size at typical heating conditions in the DLR V2G hypersonic low density tunnel [5]. Requirements are:

- Penetration time of a heat input shall be much shorter than the heating time.
- Heat losses due to conduction and radiation must be much smaller than heat input to be measured.

Thus the Fourier number based on test time and the Biot number [6] for the heating process must full fill the following requirements:

$$Fo = at^2 \gg 1 \text{ and } Biot = hl/k < 1 \quad (1)$$

Fig. 1 shows the basic solid and hollow model shapes with the dimensional envelope.

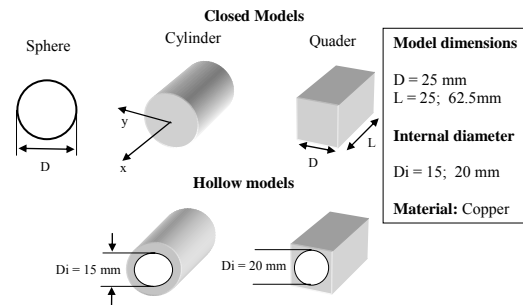


Figure 1. Survey on basic model geometries

In total 23 models have been manufactured from electrolytic copper and instrumented with two thermocouples for temperature measurement. A third thermocouple served to control the temperature of the thin walled stainless steel model support, which ensured low thermal losses. Fig. 2 shows a photograph of the complete model assembly. The following two series of models have been manufactured:

- Series A: Support from the base. Suited only for distinct angle of attack between $-90 < \alpha < 90$.
- Series R: Support on lateral side. Suited for continuous rotation and all angle of attacks.



Figure 2. Photo of all solid copper heat transfer models

2.1 The test facility and test procedure

Tests were conducted in the second test section of the DLR Göttingen vacuum wind tunnel V2G [5]. The tunnel has a circular test section with 0.4 m diameter and allows continuous operation with a Mach 20 flow. The double model injection system, sketched in Fig 3, required a modification for continuous model rotation.

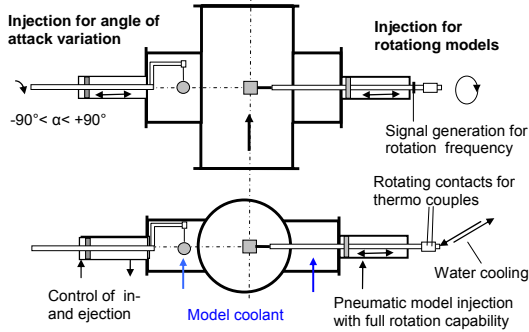


Figure 3. Double model injection with control elements

After the tunnel has reached its nominal flow state the following procedure can be applied:

- Reference sphere injection from the left chamber
 - Injection of the test model from the right chamber
- After each test the model is ejected and cooled down for a new measurement with different angle of attack α . Thus angle of attacks between $\alpha = 0^\circ$ and 90° could be tested during one tunnel run.

2.2 The flow conditions and data evaluation

As the shape dependence of heat transfer was of primary interest, all tests have been conducted at one flow condition shown in Tab. 1.

Table 1. Test conditions in the V2G tunnel

Stagnation pressure P_0	bar	30
Stagnation temperature T_0	K	1200
Pitot pressure in test section p_{t2}	mbar	0.897
Mach number Ma		25.94
Reynolds number Re_0/L	1/m	266.34

During each test the temperature history $T(t)$ of the model temperature was recorded on a laptop with data acquisition system. Fig. 4 shows a typical record.

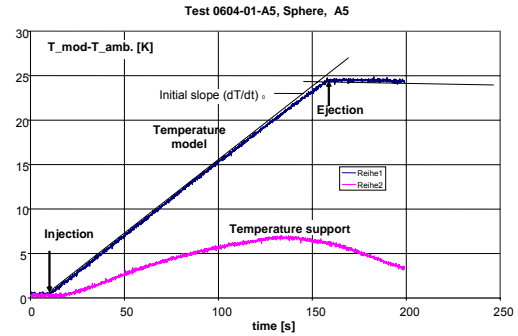


Figure 4. Typical recorded temperature time history

Immediately after injection we observe a linear increase of the model temperature with time. Test duration was 150 seconds, which resulted in a temperature increase of 25 K. After ejection the extreme small temperature decrease with time indicates that heat losses during the test time can be neglected.

From the time history and the calorimetric constant WK of the model the integral heating rate Q' can be deduced. For an isothermal model with negligible heat losses the evaluation reduces to

$$Q' = WK \left(\frac{dT}{dt} \right) \quad (2)$$

Q' integral heat transfer to model, J/s

WK calorimetric model constant, J/K

dT/dt slope of temperature time record

For each model test the following data have been evaluated for angles of attack between $\alpha = 0^\circ$ and 90° .

Heat flux to model using the frontal area at $\alpha = 0^\circ$ as reference:

$$q'(\alpha) = Q'(\alpha)/A_{ref} \quad (3)$$

Heat flux normalized with value at $\alpha = 0^\circ$:

$$q'(\alpha) / q'(\alpha=0^\circ) \quad (4)$$

For rotating models the mean heat flux during one rotation is evaluated. In total more than 200 individual heat transfer tests have been conducted on the 21 models

2.3 Test results

Fig. 5 shows for the model A6 and R4 the normalized heat flux distribution as function of angle of attack. Model A6 had a support from the back and R4 had a lateral support and could also continuously be rotated. With increasing angle of attack α the heat flux increases due to larger flow exposed area. Heat flux reaches a maximum at $\alpha \approx 60^\circ$. At $\alpha \approx 90^\circ$ the model support on the base increases the heating on the A type model. Model R7 is similar to R4 however the rotation axis is

now the main body axis. Test results of this model are shown in Fig. 6.

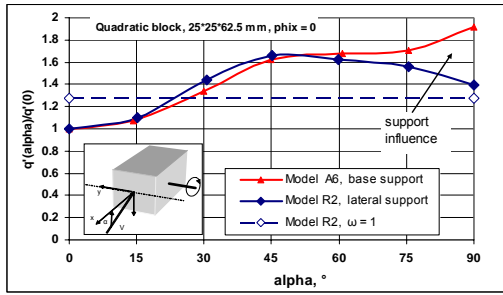


Figure 5. Normalized heat transfer on Model A6 and R2

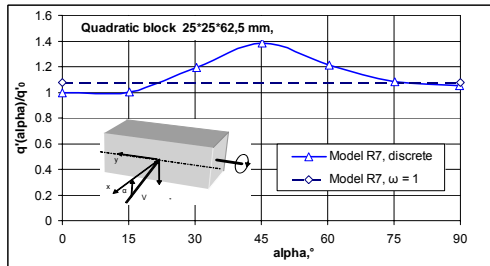


Figure 6. Normalized heat transfer on model R7

On this model we observe the highest heating at $\alpha = 45^\circ$, with the 90° corner pointing in flow direction. The heat flux behavior for a rotation axis through the diagonal is shown in Fig. 7. We observe the highest heat transfer at $\alpha = 90^\circ$. This orientation corresponds to $\alpha = 45^\circ$ for rotation around the central axis shown in Fig. 6.

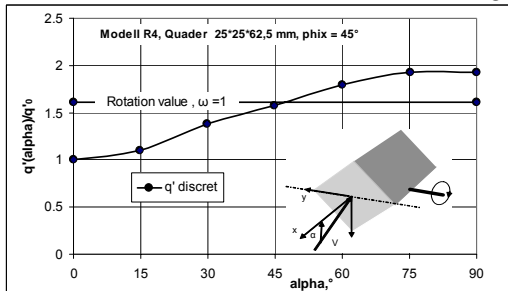


Figure 7. Normalized heat transfer on model R4

The influence of a hole on the heating becomes clearly evident by comparison of solid and hollow models. Fig. 8 shows for the solid R6 and the hollow R11 cylinder the integral heating rate Q' . At $\alpha = 0^\circ$ the hollow cylinder has a 40 % higher heating as the solid one, which is primarily caused by flow through the hollow cavity. The heating of the hollow cylinder shows no strong dependence on angle of attack. This means that the increased heating on outer surfaces is compensated by the reduction of internal heating. On the solid cylinder we observe again the strong increased heating between $\alpha = 0$ and 45° and the leveling off to almost constant values between $\alpha = 45$ and 90° . The rotation

averaged heating rates, represented by dashed lines, show the remarkable effect that during one rotation period both cylinders receive almost identical heat input.

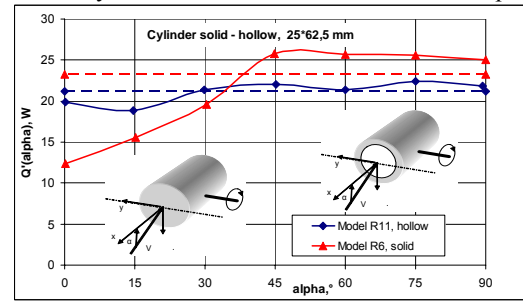


Figure 8. Heating rate of solid and hollow cylinder

2.4 Comparisons with SCARAB heating formula

The aerodynamics of SCARAB is based on local panel methods [3]. This means that for each elementary surface panel the pressure p , shear stress τ and heat transfer rates q' are calculated. The integration over all surface elements gives then the integral aerodynamic forces and heating rate. SCARAB distinguishes between free molecular, transitional and continuum heating rates. In transitional flow SCARAB uses a bridging method. The comparison between experimental data of the R3 model with numerical results calculated with SCARAB bridging shows in Fig. 9 a reasonable agreement.

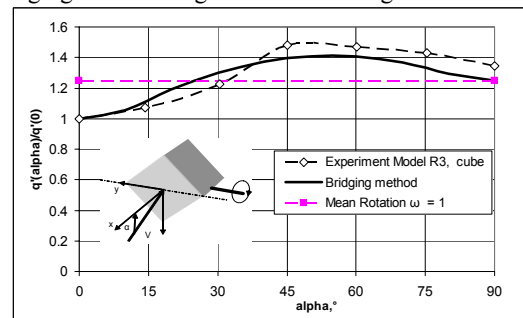


Figure 9. Experimental data versus bridging method prediction for model R3

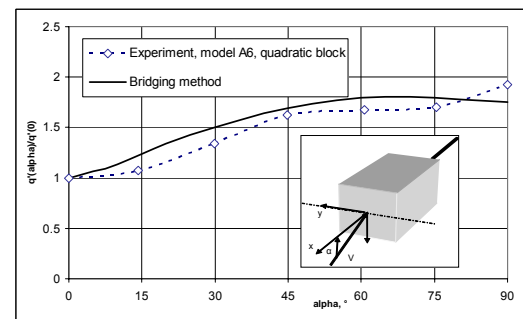


Figure 10. Experimental data versus bridging method prediction for model A6

Fig. 10 compares the experimental results of model A6 (long quadratic block) with the prediction of the bridging method. Again reasonable agreement is evident.

2.5 Summary of heat transfer measurement

The heat transfer tests with 22 different geometric models provide a valuable database for the dependence of the integral heating rate on body shape and angle of attack.

The test setup for rotating models needed a rotating water supply to cool the model support and a rotating feed out of the thermocouple signals. The new support for rotating models worked reliable, however during some tests the thermocouple signals have been influenced and showed some unexplained nonlinearity.

Selected heating results on solid bodies have been compared with the SCARAB analysis. The angle of attack dependence of the heating rates $q(\alpha)/q(\alpha=0^\circ)$ is reasonably predicted with SCARAB methods.

All tests have been conducted at one flow condition in the slip flow regime. Thus the change of heating rates with Reynolds number was not investigated

3. MATERIAL DESTRUCTION TESTS

These tests were conducted in the arc jet facility L2K of DLR Cologne [7]. Main objective of these tests was to investigate the destruction behavior of multilayer CFRP structures, whose use in S/C and launcher upper stages is continuously increasing.

The tests in the L2K were performed at simulated re-entry conditions shown in the following Tab. 2. The table shows that atomic oxygen and molecular nitrogen are the main constituents of the test section flow.

Table 2. Test section conditions in the L2K

Parameter	Dimens.	Value
Cold wall heat flux q'	kW/m^2	1310
Specific enthalpy h_0	MJ/kg	8.6
Total temperature, T_0	K	4356
Test section Pitot pressure p_{t2}	hPa	1.65
Free stream density ρ	kg/m^3	$6.7 \cdot 10^{-4}$
Free stream temperature T	K	730
Mach number	Ma	5.2
Mole fraction O	n_{O}	0.291
Mole fraction O2	n_{O_2}	0.0216
Mole fraction N2	n_{N_2}	0.659
Mole fraction N	n_{N}	$<10^{-4}$

3.1 The test models

All test models were made as cylindrical samples with 50 mm diameter and a thickness between 12 and 60 mm. The models were mounted on a water cooled injection system with support from the back.

The following Fig. 11 shows the basic model holder with the Titanium model no. 12.

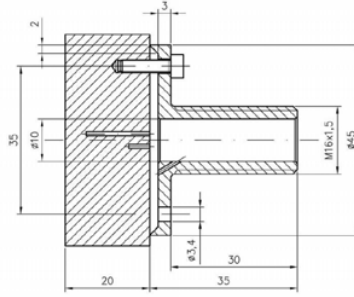


Figure 11. Model holder with solid Titanium model

Into the two visible holes in the solid titanium disk two thermocouples have been inserted one 5 mm behind the front face and one 5 mm in front of the back side. All other models have also been instrumented with two thermocouples mounted in different depths.

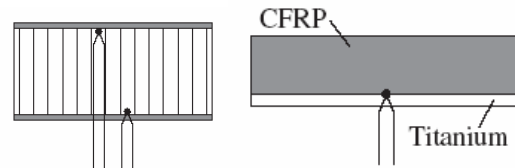


Figure 12. Thermocouple positions in different model types (e.g. Honeycombs, Ti with CFRP)

As the destruction of honeycombs with CFRP face-sheets is connected with many uncertainties, a series of such elements was tested. Original HC samples have been provided by S/C manufacturer and used for preparation of the test models. The following table lists the model numbers and names given according to S/C origin and typical construction characteristics.

Table 3. Summary of models for destruction tests

N o	Model name	Facesheet Mat. s, mm	HC	S _{HC} mm
1	Sylda-Cyl-1.1	Vicotex 0.7	Al	15
2	Sylda-Cyl-1.2	Vicotex 0.7	Al	15
3	Sylda-Cyl-2.1	Vicotex 0.7	Al	15
4	Sylda-Cyl 2.2	Vicotex 0.7	Al	15
5	Sylda-Cone-1.1	Vicotex 0.8	Al	15
6	Sylda-Cone-1.2	Vicotex 0.8	Al	15
7	Sylda-Cyl/Cone	Vicotex 1.5	Al	15
8	GOCE Solar	CFRP 0.4	Al	64
9	GOCE CC-HC	C/C, 1.7	C/C	37
11	Glass-Fiber HC	GF/Epoxy 0.4	Al	12.3
10	GOCE-CC	C/C 3.2mm		
12	Titanium	solid 20 mm		
13	Ti-CFRP	Ti 1.5mm CFRP 7.5 mm		

The honeycomb model No.1 (Sylva-Cyl-1.1), before mounting on the model injection holder, is shown in Fig. 13. The lateral cylindrical surface of the honeycomb is covered by several CFRP layers. This protects the internal HC structure against direct heating.



Figure 13. Model No.1 before testing

Fig. 14 shows the model no. 2 mounted on the injection support.



Figure 14. Model No. 2 on support before testing

After the tunnel has reached its operational condition the models are injected into the flow and the destruction behaviour is registered and observed by video.

The following data have been recorded during each test:

- Video sequence of destruction
- Temperatures of the two thermocouples
- Front surface temperatures measured with two Pyrometers

3.2 Typical measurement results

We show the observed destruction behaviour for model No. 1 (Sylva honeycomb) and Model No.13, which was a 1.5 mm thick titanium plate protected with 28 CFRP layers. Model No.13 represents in principle the construction of a thin walled titanium tank reinforced by many layers of CFRP.

Typical honeycomb detraction

Fig. 15 shows the Sylva Cyl-1.1 (Model No.1) 12 seconds after injection during the main destruction process. The recorded temperatures are shown in Fig. 16. Thermocouple TC1 behind the first facesheet reaches a temperature of 1600 K and is destroyed after the facesheet at 13 seconds. The second thermocouple TC2 located at

the back facesheet is destroyed about 5 seconds later. Then the temperature in the model holder starts to increase. The pyrometer signal show immediately after injection a surface temperature on the first facesheet of 2000 K. After destruction of this facesheet the surface temperature shows random fluctuations, which are associated with destruction of the aluminium honeycomb. Thus after 30 second of exposure time the CFRP honeycomb elements are completely destroyed.

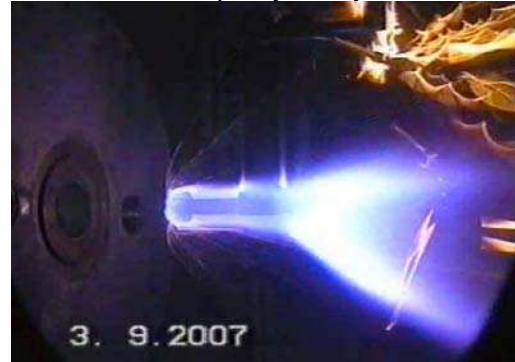


Figure 15. Model No.1 at 12 seconds after injection

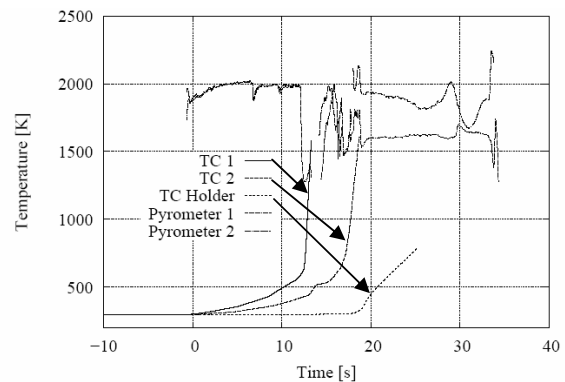


Figure 16. Model 1 recorded temperature histories

The model after testing is shown in Fig. 17. Only the lateral protective CFRP cover survived. The complete honeycomb with both facesheets has been destroyed.



Figure 17. Model No. 1 after test exposure

Destruction CFRP reinforced titanium, Model 13

This model should represent a structural element of an high pressure titanium tank reinforced with external CFRP layers. Fig. 18 shows the model before and Fig. 19 during the test. The bright traces in Fig. 19 are generated by hot carbon fiber elements released during the ablation process.

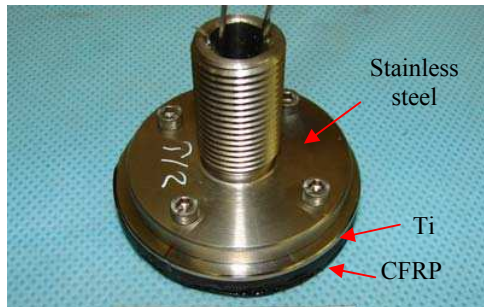


Figure 18. Model 13, 1.5 mm Titan and 7.5 mm CFRP

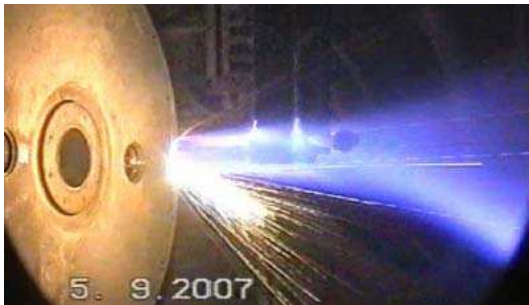


Figure 19. Model No. 13 during test at $t = 11.8$ s

Fig. 20 contains the recorded temperature time history of the test. Pyrometers show that the CFRP surface reaches after few seconds a temperature of 2000 K. This temperature remains constant for 210 seconds. During this time also a continuous ablation of CFRP can be observed. Thermocouple TC 1 is located at the interface CFRP/Ti 7.5 mm behind the original surface. Due to the protective action of the ablating CFRP the temperature at this position increases very slowly and reaches at $t = 175$ s the melting state of the TC, which is indicated by loss of signal. The holder temperature shows before test end a strong temperature increase. Also pyrometer temperatures show at this time some fluctuations. At this time also a loss of liquid metal droplets could be observed.

Inspection of the model after the test, Fig. 21, showed: On the central region of the model part of the CFRP structure survived the test. From lateral side the Titanium and the stainless steel support started to melt. The model after the test had not only recessed CFRP but also a smaller irregular external diameter due to Ti and stainless steel melting. We suppose that before end of

the test titanium started to melt behind the thin 2000K hot CFRP layer and from the unprotected lateral side.

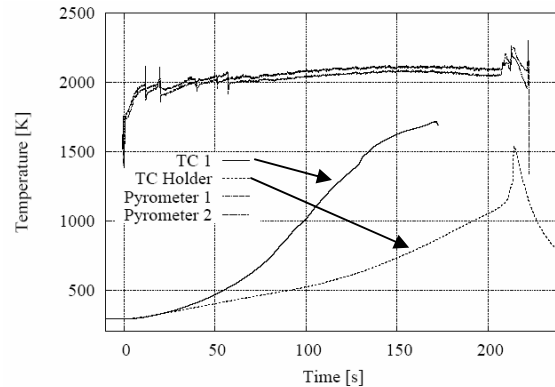


Figure 20. Mode 13 recorded temperature histories



Figure 21. TI/CFRP model after 220 s test time

3.3 SCARAB simulations of destruction tests

In order to compare the arc jet measurements with SCARAB results, numerical simulations have been conducted. For these simulations SCARAB was used in an experimental 'wind tunnel mode'. This mode deactivates the flight dynamic module. Thus the modelled geometry remains in a fixed dynamic state (velocity, altitude). The modules for aero-heating, thermal analysis and melting analysis including material database remain active.

Primary objective for the SCARAB wind tunnel mode was to reproduce the wind tunnel conditions, which primarily concern the acting heat flux. Tab. 2 with L2K test conditions shows that arc jet simulates primarily the conditions behind a shock wave and not the static free stream condition in the atmosphere. This is due to chemical relaxation phenomena during nozzle expansion. This becomes also clear if we compare static temperature and chemical composition in the arc jet. The test section free stream is characterized by high static temperatures and strongly dissociated oxygen. Thus for the SCARAB wind tunnel mode a flight condition was selected, which reproduces the heat flux value. The

following Tab. 4 compares the corresponding conditions based on heat flux duplication.

Table 4. SCARAB W-T mode versus L3K conditions

Parameter		SCARAB	L2K
Geodetic altitude	Z [km]	53.596	-
Free stream (flight) velocity	v_∞ [m/s]	3606	3093
Free stream density	ρ_∞ [kg/m ³]	$6.7 \cdot 10^{-4}$	$6.7 \cdot 10^{-4}$
Free stream static pressure	p_∞ [hPa]	0.51	1.65
Free stream static temperature	T_∞ [K]	264.6	730
Cold wall heat flux	\dot{q}_c [kW/m ²]	1379	1380*
Specific enthalpy	h_0 [MJ/kg]	6.8	8.6
Mach number	Ma [-]	11.1	5.2 [†]
Pitot pressure	p_{t2} [hPa]	44.1	61 [†]
Adiabatic exponent	κ [-]	1.4	1.42 [†]
Mole fraction O	n_O [-]	0.001	0.291
Mole fraction O ₂	n_{O_2} [-]	0.209	0.0216
Mole fraction N	n_N [-]	-	$< 10^{-4}$
Mole fraction N ₂	n_{N_2} [-]	0.781	0.659
Mole fraction NO	n_{NO} [-]	-	0.0306
Mole fraction Ar	n_{Ar} [-]	0.009	-

Selected wind tunnel models were modeled in SCARAB with their original geometry and material. Model support was not included in the SCARAB model. In order to account for heat conduction the, cylindrical models were generated as a set of circular disks (~ 20 disk sheets for a 20 mm thick model)

Fig. 22 shows the calculated temperature distribution in the solid Titanium model after 70 S of heating.

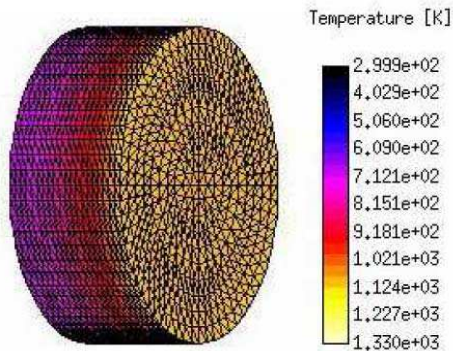


Figure 22. Temperature in titanium model 12 at 70s

In Fig. 23 we compare the SCARAB calculated temperature time profiles with the measurements for the titanium model 12. The SCARAB surface temperature follows initially the pyrometer temperature and reaches a maximum constant value of 1550 K. At $t = 60s$ pyrometer temperatures jump to 1800 and 2000 K, which we attribute to a surface oxidation and change of emission coefficient. This was confirmed by model inspection after the test, which showed a colored titanium surface and no melting. The internal temperatures of SCARAB analysis reach 1550 K at position of 5 mm and 1200 K at 15 mm behind the original surface. The thermocouple measurements show initially a slower

response and the signals break down at $t = 100s$ when melting temperature of the thermocouples is reached.

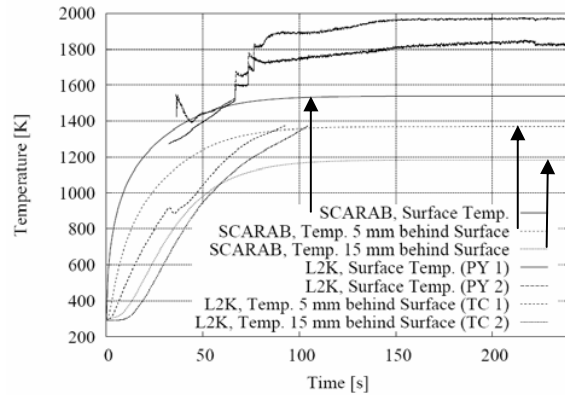


Figure 23. Model No.12 Ti, Test results versus SCARAB

The test and SCARAB analysis shows no mass loss of titanium. Inspection of the model after the tests showed that the surface was covered by a colored oxidation layer.

In Fig. 24 we compare the SCARAB analysis with arc jet data obtained on model 13, the CFRP protected titanium plate.

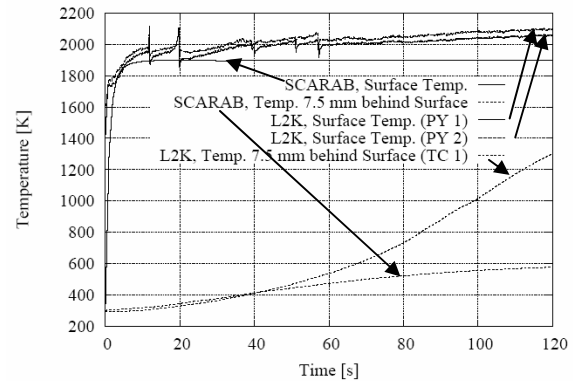


Figure 24. Model No. 13 Ti covered with CFRP, Test results versus SCARAB

Surface temperature calculated with SCARAB increases very rapidly and reaches a constant value of 1900 K, which is about 200 K below the pyrometer data PY1 and PY2. The temperatures at the interface CFRP-Titanium, which is 7.5 mm behind the original surface agree for the first 50 seconds very well. After this time the SCARAB predicted temperature increase with time is much smaller as recorded test data. We attribute this to different modeled heat conductivity with temperature

In conclusion we have to state that the SCARAB wind tunnel mode is a very attractive method to directly calibrate important code elements against test results in ground facilities.

4. CONCLUSIONS

Wind tunnel and arc jet tests offer an excellent possibility to validate distinct analysis modules of codes for re-entry destruction prediction.

The heat transfer tests with 22 different geometric models provide a valuable database for the dependence of integral heating rate on body shape and angle of attack. Selected heating results have been compared with the SCARAB analysis method and reasonable agreement could be found.

Material destruction tests have been conducted with 14 samples under re-entry heating conditions of 1400 kW/m² in the L2K arc jet facility of DLR.

Major part of the models (7) were original aluminium honeycomb samples with CFRP facesheets from Ariane-5 payload adapter Sylda. Two other samples were special carbon-carbon materials used within the gradiometer of GOCE.

The other samples represented solid titanium alloy and titanium CFRP reinforced tank elements.

The destruction behaviour of all honeycombs is very similar and determined by destruction of the first face-sheet. However a wide span of failure times between 1 and 27 s could be observed.

The carbon/carbon material proved to be extremely resistant with small ablation rates between 0.1 and 0.2 g/s. On the plain Titanium model no melting could be observed during a test time of more than 200 s and surface temperatures close to 2000 K. This might be a result of surface oxidation and of reduced cold wall heat flux due to high surface temperatures.

For comparison of wind tunnel results with numerical simulations a SCARAB 'wind tunnel mode' has been prepared. In this mode the test samples are modelled in SCARAB and exposed to a SCARAB generated wind tunnel flow reproducing the heating rate.

The conclusions from these comparisons are that there is a reasonable agreement concerning prediction of the general destruction sequence. There are however often large differences in details of temperature evolution or exact time sequence reproduction.

These disagreements are results of:

- Insufficient modelling of chemical reactions and the ablation process
- Incorrect radiative heat loss for layered models
- Temperature dependence of thermal properties

In conclusion the SCARAB 'wind tunnel mode' is in an early experimental state and should be further improved. Possible applications are:

- Code module validations against experimental wind tunnel or arc jet tests.
- Test bed for new analysis methods

5. REFERENCES

[1] Koppenwallner G., Fritsche B., Lips T., Klinkrad H. SCARAB a Multi-Disciplinary Code for Destruction Analysis of Space-Craft during Re-entry 5th Europ. Symp. on Aerothermodynamics for Space Vehicles Cologne, Nov. 2004; ESA SP-563 pp.281-288

[2] Lips T., Fritsche B., Koppenwallner G. On-ground Risk Assessment Software for Re-entering Spacecraft. In Proceedings of the First IAASS conference, pages 191-196, Noordwijk, Netherlands, 2005 ESA Publication Division

[3] Lips T., Koppenwallner G. Re-entry Windtunnel Tests and ORSAT/SCARAB Comparisons 2007, DLR Contract 50 JR 0684, HTG Report 08-01, HTG, Katlenburg-Lindau, 2008

[4] Koppenwallner G. Kraft und Wärmeübergangsmessung in Hyperschallströmung geringer Dichte, 9. Lehrgang für Raumflugtechnik, Beitrag No.10, Göttingen 1971

[5] Hefer G. Die zweite Meßstrecke des hypersonischen Vakuumwindkanals der AVA, Baubeschreibung und Betriebsverhalten, AVA Bericht 69A 37, Aerodynamische Versuchsanstalt Göttingen, 1969, also DLR-FB 70-42, 1970

[6] Bennet C.O., Myers J.E. Momentum, Heat, and Mass Transfer, McGraw-Hill Chemical Engineering Series, McGraw Hill, 1974, USA

[7] Gülhlan, A. Arc Heated Facility LBK as Tool to Study High Temperature Phenomena at Re-entry Conditions, DLR IB-39113 -97A05, 1997

Acknowledgments:

This study was supported by:

*German Ministry for Education and Science (BMBF)
DLR Contract 50 JR 0684*

HTG highly appreciates:

*a. Support of the wind tunnel teams of
Carl Dankert at DLR Goettingen,
Ali Gülhlan at DLR Cologne*

*b. Supply of materials for model manufacture by
Marc Toussaint, ESA, Paris
Andrea Allasio, Thales Alenia Space, Torino*